ELSEVIER

Research Article

nanomedicine
Nanotechnology, Biology, and Medicine

nanomedjournal.com

Ultradeformable archaeosomes as new topical adjuvants

Leticia H. Higa, MS, Priscila Schilrreff, MS, Ana Paula Perez, PhD, Maiara A. Iriarte, MS,
Diana I. Roncaglia, PhD, Maria Jose Morilla, PhD, Eder L. Romero, PhD*

*Programa de Nanomedicinas, Departamento de Ciencia y Tecnología, Universidad Nacional de Quilmes, Roque Saenz Peña 352,
Bernal, B1876 BXD, Buenos Aires, Argentina*

Abstract

Ultradeformable archaeosomes (UDA) are vesicles made of soybean phosphatidylcholine (SPC), sodium cholate (NaChol) and polar lipids from *Halorubrum tebenquichense* (3:1:3 wt/wt). Although ultradeformable liposomes (UDL, made of SPC and NaChol at 6:1 wt/wt) and UDA were neither captured nor caused cytotoxicity on keratinocytes, UDA was avidly captured by macrophages, their viability being reduced by 0.4-1.6 mg/mL phospholipids by 25 to 60%. Instead, UDL were poorly captured and caused no toxicity. Balb/C mice immunized by the topical route with four doses of ovalbumin (OVA)-loaded UDA, at 75 μg OVA/600 μg phospholipids (125 nm mean size and -42 mV zeta potential), induced IgG titers tenfold to 100-fold higher than those immunized with OVA-loaded UDL at the same dosage. Both matrices penetrate to the same skin depth (nearly 10 μm after 1 hour on excised human skin), being the higher topical adjuvancy and higher phagocytic uptake of UDA related to its glycolipid content.

From the Clinical Editor: This work summarizes key findings related to the development of ultradeformable archaeosomes as vehicles utilized in transdermal delivery systems with improved skin penetration.
© 2012 Elsevier Inc. All rights reserved.

Key words: Vesicles; Skin; Topical adjuvants

The skin is rich in potent antigen-presenting cells (APC),[1] that are not readily accessible to parenteral vaccination except by intradermal route, which is difficult to practice.[2,3] In that sense, the topical route is an attractive alternative enabling a much closer access to the skin APC.[3,4] Topical vaccination has advantages over injectables, such as increased patient compliance,[3,5] the reduced potential reinfection by contaminated material, and waste of disposable material, as well as the need for specialized trained personnel and sterilized materials, and maintenance of cold chain.[6] These advantages are partly outweighed by dose variability and the need for strong immunomodulators, namely bacterial ADP-ribosylating exotoxins (cholera toxin, heat-labile enterotoxin from *Escherichia coli* [*E. coli*] and their mutants).[6]

Particulate and especially nanoparticulate material, when phagocytosed by immature APC, induce stronger antigen (Ag)-specific systemic humoral, cellular, and memory responses as well as mucosal immunity than soluble Ag does.[3,7] However, the stratum corneum (SC) is the main impediment for topical delivery of nanoparticulate material to skin APC,[3] and the previous disruption of a substantial SC area by mechanical, chemical, or physical means such as hydration, tape stripping, electroporation, or abrasion is required.[6] In addition, upon disruption keratinocytes induce pro-inflammatory cytokines that recall an adaptive immune response by stimulating the maturation and migration of Langerhans cells.[2,8] Topical biodegradable and nonbiodegradable polymeric and metallic nanoparticles (NPs), solid lipid NPs, and liposomes have rendered successful preclinical results.[3,9] Some of these approaches are already in advanced clinical studies.[10,11]

Archaeosomes are vesicles enclosed by one or more bilayers prepared with Total Polar Lipids (TPL) extracted from microorganisms that belong to the domain Archaea. Both in vitro and in vivo, archaeosomes are more avidly internalized by macrophages and APC than liposomes are.[12,13] They also differ from liposomes in that the inclusion of immunomodulators such as lipopolysaccharides, their synthetic derivatives, or CpG motifs within lipid bilayers is not needed to improve the adjuvancy

beyond that of a simple depot effect.[14] Unlike live vector vaccines, the priming efficiency of archaeosomes is unaffected by preexisting host inflammation due to infections.[15] Thus archaeosomes could be used in vaccination routes that mediate a direct Ag delivery to skin APC, such as the intradermal and topical routes, where adjuvants that induce neither local inflammatory foci nor any long-lasting Ag depot are preferred.[16,17]

Thus far, the adjuvancy of archaeosomes (excluding Ca^{+2} bridged archaeosomes used to stimulate the nasal mucosa of mice)[18] was assessed by parenteral but not by topical route. Our group has previously described the archaeosomes from the hyperhalophile *Halorubrum tebenquichense* at inducing Ag-specific humoral and memory responses upon subcutaneous (sc) administration in mice.[19] To enable their use as topical adjuvant, we prepared ultradeformable archaeosomes (UDA) possessing a lipid matrix made of TPL from *H. tebenquichense* rendered ultradeformable after the addition of sodium cholate (NaChol) and soybean phosphatidylcholine (SPC). According to the nature of its payload, topical UDA overcame the performance of ultradeformable liposomes made of SPC and NaChol in inducing or in delaying a systemic humoral response. Both effects presumably depended on its high and selective uptake by skin phagocytes. After dropping a few milliliters on the backs of mice in nonocclusive conditions, UDA induced systemic Ag-specific humoral responses, in the absence of visible inflammation or the need for SC disruption.

Methods

Materials

SPC (phospholipon 90 G, purity > 90%) was a gift from Nattermann Phospholipis GmbH, Cologne, Germany. Sodium cholate (NaChol), 1,2-Dimyristoyl-*sn*-glycero-3-phosphoethanol-amine-N-(Lissamine™ rhodamine B sulfonyl) (Rh-PE), Sephadex G-50 and G-75, 5(6)-carboxifluorescein (CF), ovalbumin grade V (OVA), 3-(4,5-dimethylthiazol-2-yl)-2,5-diphenyl tetrazolium bromide (MTT), aluminiumnitrat nonahydrat (Al(NO$_3$)$_3$ × 9H$_2$O) and Morin (2′,3,4′,5,7-pentahydroxyflavon, $C_{15}H_{10}O_7$ × 2H$_2$O) were from Sigma-Aldrich, St. Louis, Missouri. The fluorescent probe 8-hydroxypyrene-1,3,6-trisulfonic acid (HPTS) was from Molecular Probes (Eugene, Oregon). Sodium alendronate (ALN) was a gift from Gador, Buenos Aires, Argentina. All other chemicals and reagents were of analytical grade.

Archaebacteria growth, extraction and characterization of total polar lipids

Halorubrum tebenquichense archaeas, isolated from soil samples of Salina Chica, Península de Valdés, Chubut, Argentina,[19] was grown in 8-L batch cultures in basal medium supplemented with yeast extract and glucose. Cultures were monitored by absorbance at 660 nm and harvested in late stationary phase for storage as frozen cell pastes.

Total lipids were extracted from frozen and thawed biomass using the Bligh and Dyer method as modified for extreme halophiles and the Total Polar Lipid (TPL) fraction was collected by precipitation from cold acetone.[20] Between 90 mg and 120 mg TPL were isolated from each culture batch. The reproducibility of each TPL extract's composition was routinely screened by phosphate content,[21] thin-layer chromatography (TLC), and electrospray ionization mass spectrometry (ESI-MS). TLC plates (silica gel 60, Merck F-254, 12 × 3 cm) were run in chloroform:methanol: acetic acid: water (65:4:31.5:3.5 vol/vol/vol/vol), lipids were detected by spraying with 5% sulfuric acid followed by charring at 120°C. For negative ion ESI-MS, TPL extracts were dissolved in chloroform: methanol (1:1; vol/vol) and injected in a Thermo Finnigan LCQ Ion Max mass spectrometer (Thermo Finnigan MAT, San Jose, California) equipped with a electrospray ionization source, and interface conditions were: nebulizer gas (air) 12 μL/min, curtain gas (nitrogen), 1.2 μL/minute needle voltage of 4 kV.

Preparation of vesicles

Ternary matrix vesicles (UDA, SPC:NaChol:TPL, 3:1:3 wt/wt/wt), binary matrix vesicles (TPL:NaChol, 6:1 wt/wt), archaeosomes (ARC, TPL), ultradeformable liposomes (UDL, SPC:NaChol, 6:1 wt/wt), and conventional liposomes (L, SPC) were prepared by the thin-film hydratation method. Briefly, appropriate amounts of SPC in chloroform and TPL and NaChol in chloroform:methanol (1:1, vol/vol) were mixed in round-bottom flasks. Solvents were rotary evaporated at 40°C until elimination, and the lipid films obtained were flushed with N$_2$. Lipid films were hydrated by the addition of an aqueous phase (10 mM Tris-HCl buffer plus 0.9% wt/vol NaCl, pH 7.5 (Tris-HCl buffer)) up to a final concentration of 43 mg of phospholipids/mL. The resultant suspensions were sonicated (45 minutes with a bath-type sonicator 80 W, 40 KHz) and extruded 15 times through three stacked 0.2-, 0.1-, and 0.1-μm pore size polycarbonate filters using a 100 mL Thermobarrel extruder (Northern Lipids, Vancouver, Canada).

To prepare ALN-loaded vesicles (ALN-UDA and ALN-UDL), ALN was dissolved in the aqueous phase used for the hydration of the thin film at 30 mg/mL. After extrusion, vesicles were purified by gel filtration on Sephadex G-50 using the minicolumn centrifugation technique.[22] ALN was quantified by indirect fluorescence detection of Al^{3+}-morin complex[23] after extraction of lipids by Blight and Dyer method.[24]

To prepare CF-or HPTS-labeled vesicles, CF or HPTS was dissolved in the aqueous phase used for the hydration of the thin film at 40 mM (at this concentration the dye self-quenches) or 35 mM, respectively. After extrusion, vesicles were purified using the same protocol describe above.

To prepare OVA-loaded vesicles (OVA-UDA, OVA-UDL, OVA-L and OVA-ARC), OVA was dissolved in the aqueous phase used for the hydration of the thin film at 50, 25, 12, and 6 mg/mL. After extrusion, vesicles were submitted to five freeze-thaw cycles between −70°C and 40°C. Finally, vesicles were purified on Sephadex G-75 as stated before. The OVA/phospholipid ratio was determined by protein[25] and phospholipid[21] quantification.

To prepare Rh-PE labeled vesicles (Rh-PE-UDL and Rh-PE-UDA), Rh-PE was dissolved in chloroform, and 12.5 nmol was added to the organic solution of lipids; the thin lipid film and vesicles were prepared as state above.

To prepare double fluorescent-labeled UDA (HPTS-Rh-PE-UDA), Rh-PE was dissolved in chloroform with the lipids, and HPTS was dissolved in the aqueous phase used for the hydration of the thin lipid film. After extrusion, vesicles were purified as stated earlier.

Characterization of vesicles

Phospholipids were quantified as stated above.[21] Size and zeta potential were determined by dynamic light scattering (DLS) and phase analysis light scattering (PALS) respectively, using a nanoZsizer apparatus (Malvern Instruments, Malvern, United Kingdom). Transmission electron microscopy (TEM, JEM 1200EX II, Jeol, Tokyo, Japan) images of vesicles upon uranyl acetate staining were obtained. Images of vesicles in hydrated state were obtained by Environmental Scanning Electron Microscopy (ESEM) (Zeiss Supra 55VP Field emission scanning microscope, Carl Zeiss, AG, Oberkochen, Germany).

Measurement of deformability and retention degree of vesicles

The Deformability value (D) of the vesicles was calculated according to Van den Bergh[26] as $D = J(rv/rp)^2$, where J is the rate of penetration through a permeability barrier, rv is the size of vesicles after extrusion, and rp is the pore size of the barrier. To measure J, vesicles were extruded through two stacked 50 nm (rp) membranes at 0.8 MPa using a Thermobarrel extruder.[27] Extruded volume was collected every minute along 15 minutes, phospholipid was quantified in each fraction, and J was calculated as the area under the curve of the plot of phospholipid recovered as a function of time. The average vesicle diameter after extrusion (rv) was measured by DLS.

The Retention Degree (RD) of a hydrosoluble low-molecular-weight molecule into vesicles after extrusion through the two stacked 50-nm pore size membranes was determined using CF-loaded vesicles. Fluorescence emission intensity of CF (λ_{exc}: 492 nm, λ_{em}: 517 nm) was monitored in a LS 55 PerkinElmer luminescence spectrometer, before and after extrusion. RD was calculated as: $100 - [(I_{50} - I_0)/I_T].100$, where I_{50} was fluorescence intensity after extrusion, I_0 was fluorescence intensity before extrusion, I_T was total intensity obtained by addition of Triton X-100 at 0.1% vol/vol.

Qualitative composition of UDA

UDA lipid matrix is rich in archaeolipids bearing voluminous sulfated glycolipids head groups, and after extrusion rubbery residuum usually remains stacked onto the polycarbonate membranes. To check for the potential loss of glycolipids from membrane matrix after extrusion, the lipid composition of UDA was screened by ESI-MS. Aliquots of UDA after extrusion were dissolved in chloroform:methanol (1:1 vol/vol) and analyzed by ESI-MS in positive and negative modes as state before.

Cells

Human keratinocytes (HaCaT cells) were supplied by Dr. Salvatierra of Fundación Instituto Leloir (Buenos Aires, Argentina) and murine macrophages (J774 cells) were supplied by Dr. Petray from Servicio de Parasitología y Enfermedad de Chagas, Hospital de Niños Ricardo Gutierrez (Buenos Aires, Argentina). Cells were routinely cultured in MEM (Gibco, Life Technologies, New York) supplemented with 10% fetal calf serum (FCS), 1% antibiotic/antimycotic (PAA Laboratories GmbH, Pasching, Austria) (penicillin 10,000 U/mL, streptomycin sulphate 10 mg/mL, amphotericin B 25 µg/mL) and 2 mM glutamine, at 37°C in 5% CO_2 and 95% humidity.

Cytotoxicity

Cell viability was measured by the MTT assay and by lactate dehydrogenase (LDH) leakage in culture supernatants. HaCaT and J774 cells were seeded at a density of 3×10^4 cells per well onto 96-well flat-bottom plates and grown for 24 hours at 37°C. Then, medium was replaced by 100 µL of fresh MEM with 5% FCS containing decreasing concentrations of empty UDA/UDL or ALN- loaded UDA/UDL in a half-fold dilution series (1.6 to 0.2 mg/mL of phospholipids and 100 to 12.5 µg/mL of ALN) or free ALN (1500 to 375 µg/mL), and cells were incubated at 37°C for 24 hours.

After incubation, supernatants were transferred to fresh tubes, centrifuged at 250*g* for 4 minutes, and LDH content was measured using lactate dehydrogenase CytoTox Kit (Promega Corp., Madison, Wisconsin). LDH leakage was expressed as percentage relative to the treatment with Triton-X 100. Toxicity limit was set at 10% LDH leakage. On the other hand, 110 µL of 0.45 mg/mL MTT were added to cells attached to plates. After 3 hours of incubation, MTT solution was removed, the insoluble formazan crystals dissolved with 100 µL of dimethylsulfoxide (DMSO), and absorbance was measured at 570 nm using a microplate reader (Dynex Technologies, MRX tc, Chantilly, Virginia). Viability of cells was expressed as percentage of the viability of cells grown in medium.

Cell uptake of Rh-PE or HPTS-labeled UDA and UDL

The uptake of fluorescent labeled UDA and UDL by keratinocytes and macrophages was analyzed by flow cytometry. HaCaT and J774 cells seeded at density of 3.5×10^5 cells per well onto 6-well microplates were grown for 24 hours at 37°C. Medium was replaced with fresh MEM with 5% FCS containing Rh-PE- or HPTS- labeled vesicles at 0.2 mg/mL phospholipids and cells were incubated for 1, 3, and 5 hours at 37°C. After each incubation time, medium was removed, cells were washed with phosphate-buffer saline (pH 7.4) (PBS) and harvested by trypsinization. Cells were fixed in 1% formaldehyde at 4°C. Cells were washed, suspended in PBS, and a total of 1×10^5 cells were analyzed by flow cytometry (Becton Dickinson FACSCalibur, San Jose, California). Data were analyzed using WinMDI 2.9 software.

In vitro skin penetration of HPTS and Rh-PE labeled UDA

Excised human skin from two healthy Caucasian female patients who underwent abdominal plastic surgery was used. After excision, the skin was cut into 10×10 cm^2 pieces, the subcutaneous fatty tissue was removed using a scalpel, and the surface was cleaned with Tris-HCl buffer. Disks of 24 mm in diameter were punched out and transferred directly onto a filter paper soaked with Tris-HCl buffer and placed into the cavity of a Teflon block (Saarbrücken Penetration Model apparatus). Double

Table 1
Immunizations schemes

Route of administration	Pretreatment (days −7, −6, −5, −4, −3)	Adjuvant (50 μL)	Phospholipid dose (μg)	OVA dose (μg)	Days of immunization
Subcutaneous	No	UDA	600	600	0, 21
Intramuscular	No	Al_2O_3 (100 μg)	-	600	0, 21
Topical	No	UDA	300	75	0, 7, 14, 21
				150	
Topical	No	UDA	600	75	0, 7, 14, 21
				300	
				600	
Topical	No	UDL	300	75	0, 7, 14, 21
				150	
Topical	No	UDL	600	75	0, 7, 14, 21
				300	
				600	
Topical	No	L	600	75	0, 7, 14, 21
Topical	No	ARC	600	75	0, 7, 14, 21
Topical	ALN-UDA (300 μg phospholipid-0.2 μg ALN)	UDA	600	75	0, 7, 14, 21
Topical	ALN-UDL (300 μg phospholipid-0.2 μg ALN)	UDA	600	75	0, 7, 14, 21
Topical	ALN (75 μg)	UDA	600	75	0, 7, 14, 21
Topical	Buffer	UDA	600	75	0, 7, 14, 21

fluorescent labeled UDA (HPTS-Rh-PE-UDA) were applied to the skin surface and incubated for 1 hour at 35°C in non-occlusive conditions. Then, the skin was rapidly frozen in dry ice, embedded in OCT, and sliced in sections of 8 μm thickness perpendicular to the skin with a cryomicrotome (Reichert-Jung CryoCut 1800, Heidelberg, Germany). Skin slices were fixed with 10% formaldehyde and observed with a Nikon confocal laser microscope equipped with an Ar laser (488 nm for HPTS excitation) and a He–Ne laser (543 nm for Rh-PE excitation).

Immunization

Male 6-8-week-old BALB/c mice were housed under standard-environment conditions at 25°C, were humanely cared for and supplied with food and water ad libitum. The study was conducted following the Institutional Experimental Guidelines for Animal Studies. Five mice per group were immunized according to the schemes shown in Table 1.

Sampling and IgG titers

Blood was collected from the tail veins at weekly intervals up to 10 weeks, and IgG antibody and isotypes were analyzed by ELISA. Briefly, microtiter plates were coated overnight at 4°C with 45 μg/mL OVA in 0.1 M carbonate-bicarbonate buffer (pH 9.6) and then blocked for 1 hour at 37°C with PBS containing 0.2 % Tween 20 (0.2% PBST) after washing with 0.05% PBST. Another wash as above described was followed by the addition of 100 μL of three-fold dilutions of individual sera in 0.05% PBST. After 2 hours at 37°C and further washing, the plates were incubated for 1 hour at 37°C with horseradish peroxidase-conjugated goat anti-mouse IgG (Millipore-Chemicon International, Temecula, California) diluted 1:2000 in 0.025% PBST. To determine the antibody isotyping, horseradish peroxidase-conjugated rat anti-mouse IgG1 or IgG2a revealing antisera (PharMingen, San Diego, California),

diluted 1:1000, were used. The plates were further washed and incubated with ABTS [2, 2′-azino-bis (3-ethylbenzthiazoline-6-sulphonic acid), Sigma] for 10 minutes at room temperature (20°–25°C) in the dark. The absorbance was measured at 405 nm using a microplate reader. Antibody titers were represented as end-point dilutions exhibiting an optical density of 0.3 units above background.

Statistical analysis

Statistical analyses were carried out with the Prisma 4.0 Software (GraphPad, San Diego, California). Group means were evaluated by ANOVA with Tukey's analysis to compare individual groups; significance levels are shown in figure legends.

Results

Characterization of TPL and vesicles

Each TPL extract was routinely characterized by phosphate content, TLC and ESI-MS. A regular content of 68-μmol phosphate per 100 mg dry TPL was quantified. TLC run showed four spots of 0.13, 0.21, 0.37, and 0.74 retention factor (Rf). The ESI-MS spectrum revealed archaetidyl phosphatidylglycerol (PG, at m/z 805), phosphatidylglycerophosphate methyl ester (PGP-Me, at m/z 899), sulfated diglycosyl diphytanyl-glycerol diether (S-DGD-5, at m/z 1055), bisphosphatidylglycerol (BPG, at m/z 760-bicharged and 1521-monocharged) and monosulfated glycocardiolipin (S-DGD-5PA, at m/z 885-bicharged and 1770-monocharged) (as shown in Figure 1, E).

Aiming to achieve ultradeformable vesicles containing the highest proportion of TPL, binary (TPL:NaChol 6:1 wt/wt) and ternary (TPL:SPC:NaChol 3:3:1 wt/wt/wt) lipid matrices were prepared. Their mechanical behavior, described by the parameters D and RD, were compared with those of UDL and the non-ultradeformable L and ARC. Mean size and zeta
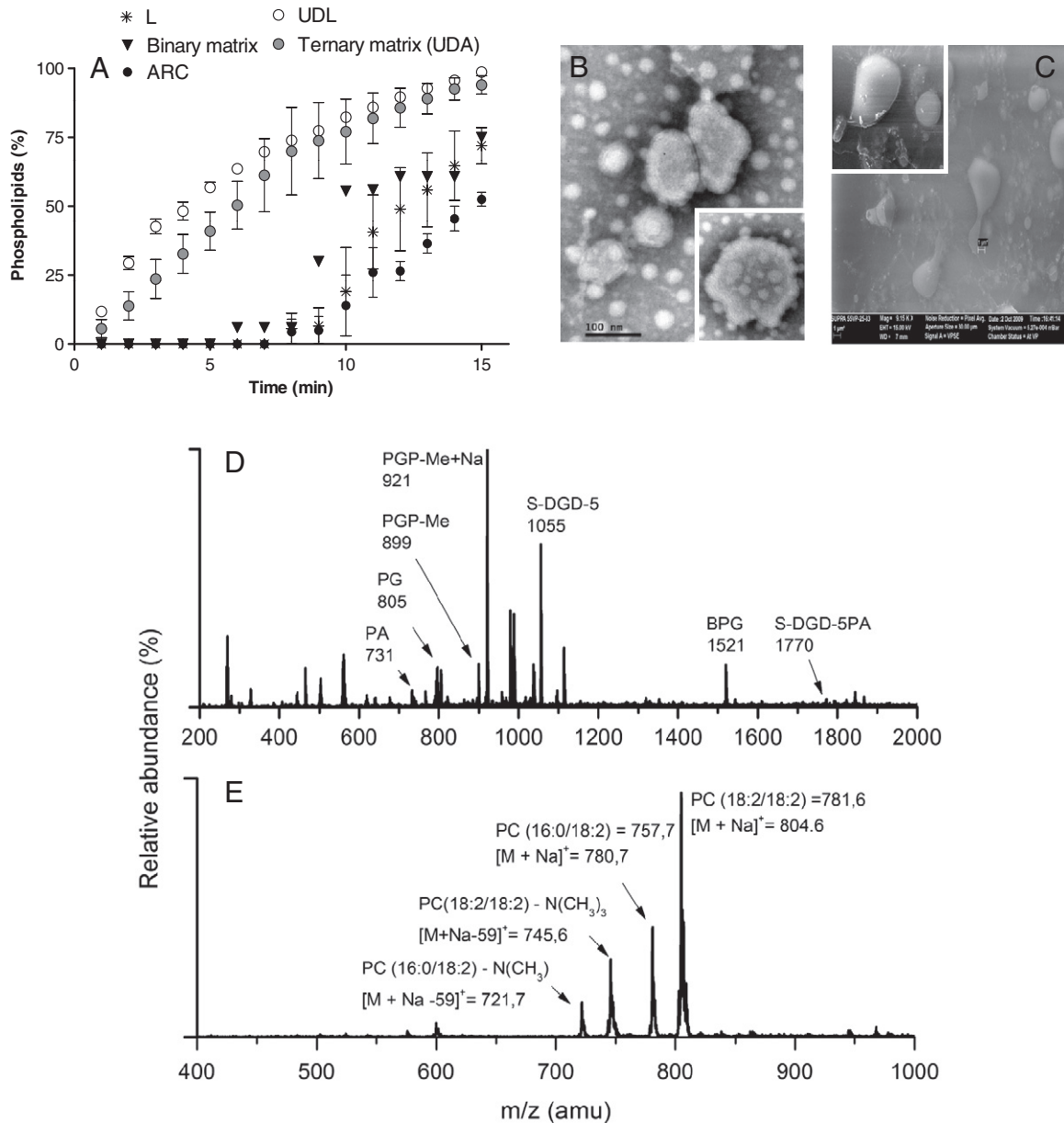
Figure 1. Characterization of vesicles. **(A)** Phospholipid passage through 50-nm pore size membranes versus time. Values represent mean ± SD (n = 3). **(B)** TEM of UDA (200,000×); inset, detailed picture showing UDA size and unilamellarity (250,000×). **(C)** ESEM micrographs of UDA; inset, detailed picture. ESI-MS spectrum of UDA in negative **(D)** and positive mode **(E)**.

potential of vesicles are shown in Table 2. Two main patterns of extruded phospholipid flux were distinguished (Figure 1, *A*). The first one was characterized by the absence of phospholipid passage during the first 5–10 minutes with a 60% recovery of phospholipids after 15 minutes, as occurred with ARC, L, and binary matrix vesicles. The second pattern was characterized by a fast passage of 75% phospholipids during the first 10 minutes, with a 95% recovery of phospholipids after 15 minutes, as occurred with UDL and ternary matrix vesicles. The calculated D values for ternary matrix vesicles were 20% lower than that of UDL (3700 vs ~4600 respectively). On the other hand, ARC, L, and binary matrix vesicles had nearly 95% lower D

values than that of UDL (~290). Ultradeformable vesicles possess not only high D values but also have high RD of hydrophilic content. This study found that the RD of CF from UDL and ternary matrix vesicles was around 90%, whereas that from L and binary matrix vesicles was nearly 4.5%. On the bases of their elevated D and RD values, only ternary matrix vesicles but not binary matrix vesicles could be defined as UltraDeformable Archaeosomes, UDA. OVA- and ALN-loaded UDA showed the same D as empty UDA. Finally, the zeta potential of L and UDL were similar in the order of −10 mV and remained unchanged after OVA loading. On the contrary, the zeta potential was reduced from ~−60 mV for

Table 2
Structural parameters of the vesicles

Sample (μg OVA–μg phospholipids)	Mean size (nm)* (Polydispersity Index)	Zeta potential* (mV)	OVA or ALN/phospholipid ratio (% wt/wt)*
Ternary matrix	108 ± 1.1 (0.313)	−50 ± 2.4	-
Binary matrix	370 ± 129 (0.780)	−45 ± 2	-
ARC	410 ± 155 (0.980)	−60 ± 5	-
UDL	105 ± 2 (0.107)	−10 ± 1	-
L	112 ± 5 (0.100)	−5 ± 0.5	-
ALN-UDA	117 ± 1 (0.112)	−39 ± 1.9	7 ± 0.2
ALN-UDL	157 ± 20 (0.212)	−7 ± 1.7	7 ± 0.3
OVA-L (75-600)	174 ± 1 (0.306)	−4 ± 0.2	16 ± 5
OVA-ARC (75-600)	425 ± 150 (0.890)	−25 ± 3	20 ± 6
OVA-UDA (75-300)	187 ± 13 (0.251)	−15 ± 2.4	16 ± 4
OVA-UDA (150-300)	240 ± 47 (0.314)	−23 ± 2.8	33 ± 10
OVA-UDA (75-600)	125 ± 24 (0.265)	−42 ± 2.0	27 ± 3
OVA-UDA (300-600)	156 ± 37 (0.332)	−41 ± 1.2	52 ± 4
OVA-UDA (600-600)	200 ± 17 (0.35)	−39 ± 1.5	100 ± 17
OVA-UDL (75-300)	150 ± 27 (0.293)	−10 ± 1.0	25 ± 10
OVA-UDL (150-300)	220 ± 37 (0.280)	−10 ± 1.2	64 ± 7
OVA-UDL (75-600)	145 ± 23 (0.275)	−11 ± 1.3	50 ± 11
OVA-UDL (300-600)	164 ± 24 (0.313)	−11 ± 1.2	75 ± 14
OVA-UDL (600-600)	186 ± 64 (0.382)	−10 ± 1.1	92 ± 13

* Values represent mean ± SD ($n = 3$).

ARC to ∼−45 mV for UDA. Besides, the OVA loading reduced the zeta potential of ARC and UDA, this last in an inverse relationship to the wt/wt % OVA. Despite that, the OVA loading did not reduce the ultradeformability of UDA or UDL; thus it was expected to have no effect on the rate and extent of skin penetration.

TEM images of UDA were unilamellar spheres of diameters close to 100 nm (Figure 1, *B*). Highly deformed, self-fused under the electronic beam (artificially enlarged) vesicles were seen by E-SEM (Figure 1, *C*).

The qualitative composition of UDA after extrusion screened by ESI-MS spectrum in negative mode, showed the conservation of the main signals of TPL (Figure 1, *D*). The signal at m/z 805 corresponded to PG, signal at m/z 899 to PGP-Me, whereas an intense signal at 921 was adjudicated to a PGP-Me and Na adduct. The signal at m/z 1521 corresponded to BPG. The strong signal at m/z 1055 was generated by S-DGD-5; meanwhile the signal was generated at 1770 by SDGD-5PA. Other minor peaks at m/z 731 (diagnostic of phosphatidic acid, PA), at m/z 407 (NaChol) and 560 and 298 (phosphatidylcholine signal) were detected as fragment ions. The ESI-MS spectrum in positive mode, showed a typical spectra of natriated phosphatidylcholine molecules (PC) $[M+Na]^+$ at m/z = 804.8 (18:2/18:2) and 780.7 (16:0/18:2) (Figure 1, *E*). At the capillary exit voltage used (4 kV), the PC mixture showed substantial fragmentation as indicated by the presence of ions resulted from loss of the group trimethylamine m/z = 59 $[M+Na-59]^+$ at m/z 745.7 and 721.7. In the positive mode, there were no archaeolipid signals.

Cytotoxicity and cell uptake

Empty UDL and UDA were not cytotoxic on HaCaT keratinocytes; only UDA reduced 25% the viability by MTT and produced 30% LDH leakage at the maximal phospholipid concentration tested (1.6 mg/mL). On J774 macrophages on the other hand, empty UDL were nontoxic, but UDA showed pronounced toxicity as the concentration was increased (Figure 2, *A* and *B*).

A similar trend that was also cell-line and lipid-matrix dependent was observed for ALN-loaded vesicles. HaCaT cells were almost refractory to ALN-loaded UDL and UDA, and to free ALN (Figure 2, *C* and *D*). On the contrary, J774 cells resulted sensitive to increased ALN-UDL concentrations, but except at the highest tested concentration, equivalent ALN-UDA concentrations caused nearly twice the damage. Remarkably, it was found that J774 cell viability was reduced 50% by free ALN at 1500 μg/mL, whereas ALN-UDL and ALN-UDA at 30- and 60-fold lower concentrations, respectively, caused a similar damage. Those results underscored a selective and higher cytotoxicity of ALN-UDA, over that caused by ALN-UDL or free ALN, on J774 cells.

Moreover, the uptake of Rh-PE- or HPTS-labeled vesicles (bilayer and aqueous markers respectively) by HaCaT and J774 cells was followed for 5 hours. In that period, the uptake of vesicles by HaCaT cells was negligible, but J774 cells captured both Rh-PE-UDA and HPTS-UDA following a lineal kinetics, at a higher rate than that of UDL (Figure 2, *E* and *F*).

In vitro skin penetration of double fluorescent-labeled UDA

Transversal cryosectioning of human skin, revealed that after 1 hour's incubation with double fluorescent-labeled UDA (HPTS-Rh-PE-UDA) the red fluorescence of Rh-PE occupied the entire thickness of SC, nearly up to 10 μm deep (Figure 3). We had previously shown that 1 hour after nonocclusive topical application, UDL lipid matrix penetrates the entire SC whereas its hydrophilic content was shuttled up to 60 micrometers below.[28] Here we observed that the matrix penetration of UDA was also accompanied by an extensive shuttling of HPTS across the viable epidermis. Taken together, this similar labels
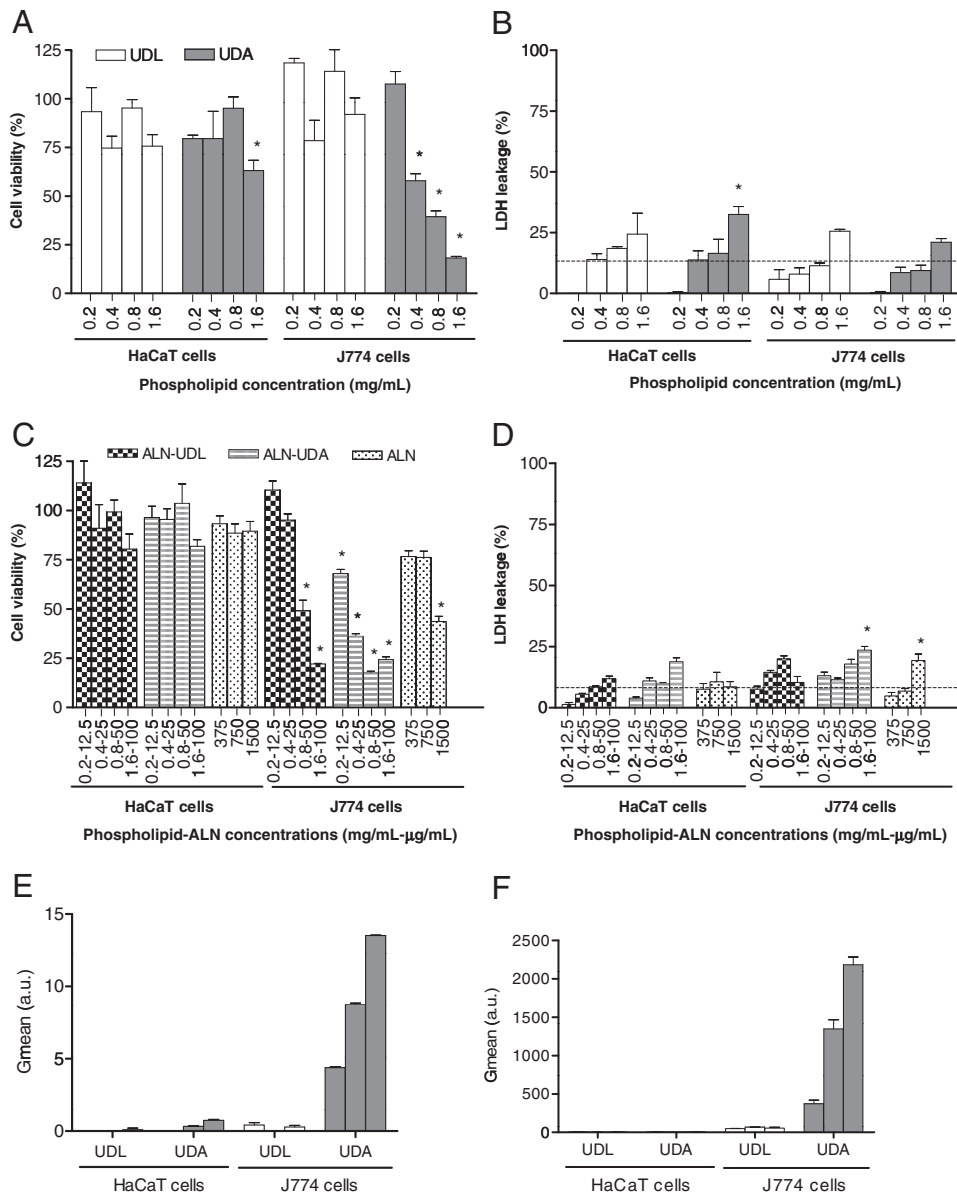
Figure 2. Cytotoxicity of empty **(A and B)** and ALN-loaded vesicles **(C and D)** on HaCaT and J774 cells upon 24 h incubation, measured by MTT **(A and C)** and LDH leakage **(B and D)**. Values represent mean ± SD ($n = 5$) *$P < 0.01$. Cell uptake of Rh-PE-labeled **(E)** and HPTS labeled-vesicles **(F)** by HaCaT and J774 cells as function of incubation time (1, 3, and 5 hrs).

distribution, plus high *D* and *RD* values, indicated that UDA and UDL had a similar mechanical behavior.

Immunization

The OVA-specific humoral immune response to topical OVA-UDA was compared with those to OVA-UDL OVA-L and OVA-ARC. The highest titers were raised by im alum adsorbed OVA, followed by those achieved by sc OVA-UDA, both used as controls (Figure 4, *A*). During the first 3 weeks, the response to sc OVA-UDA was comparable with those responding to topical OVA-UDL and OVA-UDA. After both the im and sc boost, the response was sharply

increased, to decay from day 63 on. On the other hand, after the fourth topical dose, the responses differed according to the nature of the lipid matrix: decayed to OVA-ARC, OVA-L, and OVA-UDL, but were increased to OVA-UDA. Finally, although OVA-ARC and OVA-L did not respond to the topical boost, topical OVA-UDA generated an intermediate response between the responses to OVA-UDL and sc OVA-UDA. At the current dosage, the cytotoxicity of UDA on phagocytes was not an impairment to raise topical adjuvancy.

The Ag dose is the only data reported by most of the articles on topical vaccination. Usually the antigen/carrier ratio and carrier dose are unknown. To assess whether the carrier dose
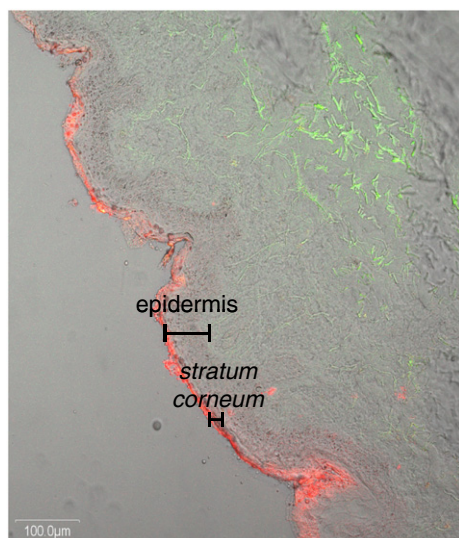
Figure 3. Representative microscope image of cryosectioned skin after incubation with double fluorescent labeled UDA (HPTS-Rh-PE-UDA). Red and green signals from Rh-PE and HPTS, respectively.

influenced the intensity of the immune response, the IgG titers were determined as a function of different OVA and lipid doses, in a series of five consecutive experiments. The response to OVA-UDA was similar at doses of 75–600 μg OVA and 300–600 μg lipid matrix; the lipid matrix at 600 μg induced earlier responses (Figure 4, *B*). The same trend was observed for OVA-UDL.

The isotype profile after topical immunizations was determined at two time points, 1 week after the last immunization and 1 week post boost. We found that OVA-L did not induce IgG2a, whereas the IgG1/IgG2a ratio to OVA-UDA was lower than that to OVA-UDL, suggesting that OVA-UDA could be responsible for a polarized Th1 response (Figure 4, *C*).

An effect associated to UDA mechanical penetration and specific composition, was the finding that pretreatment with topical ALN-UDA decreased the IgG titers and delayed by more than 2 weeks the response to OVA-UDA (Figure 4, *D*). Topical ALN-UDL and free ALN (at doses nearly 38-fold higher than that of ALN-loaded vesicles) were less efficient at decreasing and delaying the IgG titers. Bisphosphonates such as ALN, pamidronate, risedronate, and zoledronic acid induce apoptosis on phagocytic cells[29] and in particular, sc liposomal clodronate induces apoptosis/necrosis on phagocytic immature APC, such as Langerhans and dermal dendritic cells.[30] The skin immune response is recovered after migration of new cells from bone marrow, to substitute those under apoptosis.[31] Our results showed that keratinocytes neither internalized vesicles nor were affected by free ALN or ALN-loaded vesicles. On the other hand, as already reported,[29] J774 cells viability was affected by free ALN. We found here that empty UDA (and not UDL) reduced J774 viability as well, and that ALN-UDA was responsible for the highest cell damage. Hence, the decreased and delayed titers resulting after pretreatment with topical ALN-UDA, could be due to the in vivo shuttling of ALN to deeper epidermal layers, plus the toxicity of empty UDA and

ALN-UDA and these two effects could be related to mechanical penetration and specific composition of the UDA lipid matrix.

Discussion

Under nonocclusive conditions, conventional liposomes fuse and do not penetrate the intact skin mouse beyond 1-μm depth. However, the lipid matrix of UDL penetrates at least the entire depth of SC, delivering its aqueous content to the viable epidermis.[28] UDL overcomes conventional liposomes as topical adjuvants because of their special mechanical behavior or ultradeformability, gained by the presence of edge activators such as sodium cholate, polysorbates, or ethanol within the phospholipid matrix.[32,33] Only after SC penetration the UDL were lipids taken up by viable skin cells. The resultant cell response is dependent on both the chemical nature of the lipid matrix and its inner content. We found that similar to liposomes, topical archaeosomes did not penetrate the skin nor did they induce adjuvancy. Only after the archaeosomes became ultra-deformable, were these effects manifested. However, UDL and UDA manifested remarkable differences when they interacted with cells. In vitro, keratinocytes neither captured UDL nor UDA; UDA were more avidly captured by phagocytes than UDL. In vivo, topical OVA-loaded UDA induced between 10-fold to 100-fold higher systemic IgG titers than OVA-UDL. We found also that if topical vaccination was preceded by topical ALN-loaded UDA, the immune response to OVA-UDA was strongly delayed, in comparison with the less-pronounced delay caused by ALN-UDL. Because UDA had mechanical behavior that was similar to that of UDL, the differential effects had to be due to one particular or to multiple components in their TPL.

The lipids from Eukarya and bacteria domain organisms have pronounced differences in comparison with those from Archaea domain. The glycerol backbone of archaeolipids is linked by ether to saturated isoprenoid chains, mainly phytanyls and diphytanils, in an *sn-2,3* enantiomeric configuration.[34,35] After sc administration in mice, archaeosomes constitute potent adjuvants for the induction of Th1, Th2 and CD8+ T cell responses to the entrapped soluble Ag.[36-40] The mechanism responsible for adjuvancy of archaeosomes remains elusive: Archaea domain lacks lipopolysaccharides,[41] and archaeosomes from hyperthermophiles and methanogen microorganisms would not have pathogen-associated molecular patterns to serve as danger signals that activate the innate immune system.[42] Archaeosomes from *Thermoplasma acidophilum* and *M. smithii* do not appear to activate toll-like receptors 2 and 4 (lipid A-like pathways),[43] nor CD1 receptors like a-Gal glycolipids that activate natural killer cells.[44,45] However, recently it was shown that a major part of the CD8+ cytotoxic thymic lymphocyte adjuvant properties are related to the glyco-portion of archaetydil phosphate groups glycosidically linked to short oligosaccharides, like the β-(1→6) glucose-linked dimer gentiobiose.[37,46] Targeting to APC via well-known receptors such as DC-sign (Dendritic Cell-Specific Intercellular adhesion molecule-3-Grabbing Non-integrin) and the mannose receptor, by mannose-containing oligosaccharide head group formulated as archaeosomes without phosphatidyl serine (PS), was also suggested to induce both
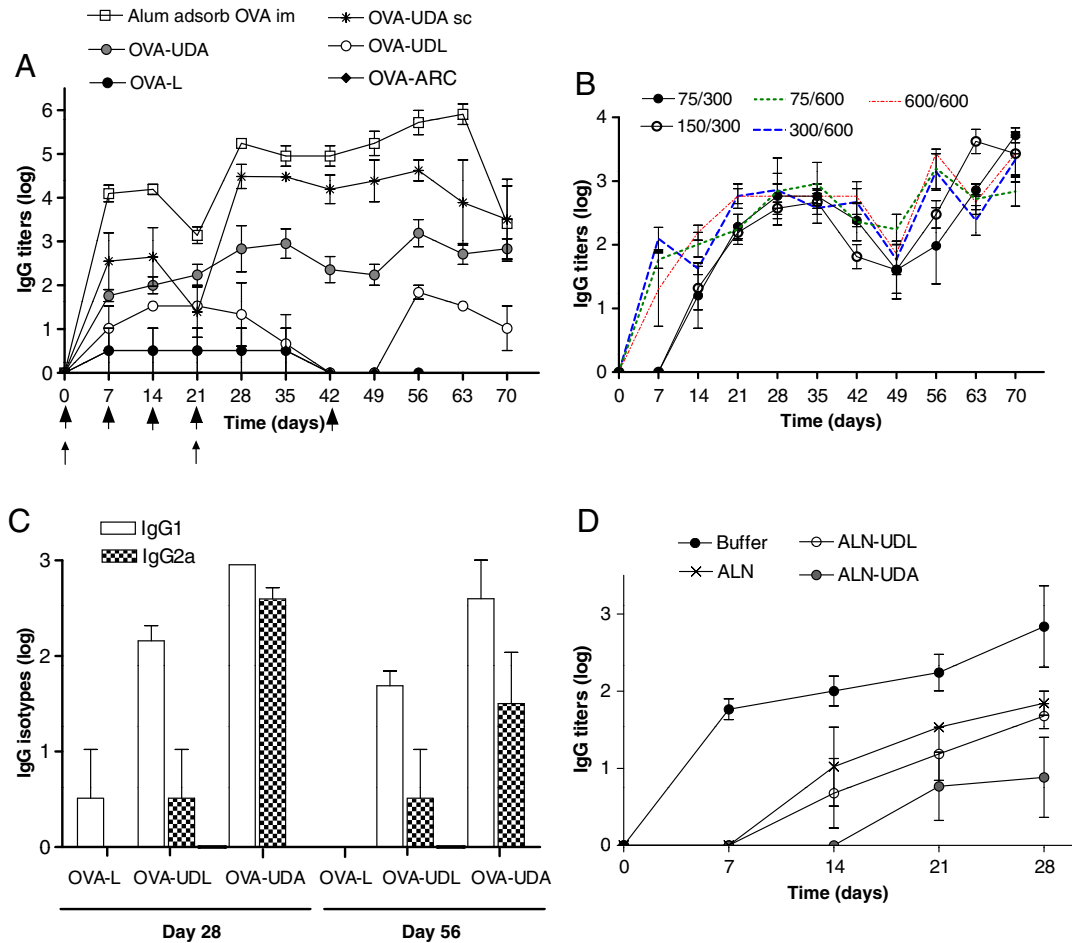
Figure 4. **(A)** Serum IgG titers after topical vesicles (75 μg OVA/600 μg phospholipids), sc and im immunization. Arrows show topical (*bold*), sc and im (*thin*) dosage. **(B)** Serum IgG titers after topical OVA-UDA at different μg OVA/μg phospholipids ratios. **(C)** IgG isotypes after topical OVA-loaded vesicles (75 μg OVA/600 μg phospholipids). **(D)** Serum IgG titers to topical OVA-UDA after topical ALN pretreatments. Values represent mean titers ± SD ($n = 5$).

targeting and cytokine upregulation.[47] The TPL from hyperhalophile archaeas such as *Halorubrum tebenquichense* have unique characteristics that vary little with gender. They lack phospholipids possessing ethanolamine, inositol, and PS, although specifically contain PG, PGP-Me, and glycosilated sulpholipids.[48] Remarkably, PG, PGP-Me, BPG, S-DGD-5, and S-DGD-5PA were the main archaeolipids composing UDA. Probably the stronger response to UDA was elicited by the presence of the mannose-containing archaeolipids S-DGD-5 and S-DGD-5PA. Hence nano-sized vesicles containing S-DGD-5 and S- DGD-5PA, capable of penetrating the intact SC to the same extent as UDL, can be highlighted as the main features of this topical adjuvant.

References

1. Banchereau J, Steinman RM. Dendritic cells and the control of immunity. Nature 1998;392:245-52.
2. Nicolas JF, Guy B. Intradermal, epidermal and transcutaneous vaccination: from immunology to clinical practice. Expert Rev Vaccines 2008;7:1201-14.
3. Combadiere B, Mahe B. Particle-based vaccines for transcutaneous vaccination comparative immunology. Microb Infect Dis 2008;31: 293-315.
4. Partidos CD, Beignon A-S, Mawas F, Belliard G, Briand J-P, Muller S. Immunity under the skin: potential application for topical delivery of vaccines. Vaccine 2003;21:776-80.
5. Clements CJ, Larsen G, Jodar L. Technologies that make administration of vaccines safer. Vaccine 2004;22:2054-8.
6. Giudice EL, Campbell JD. Needle-free vaccine delivery. Adv Drug Del Rev 2006;58:68-89.
7. Warger T, Schild H, Rechtsteiner G. Initiation of adaptive immune responses by transcutaneous immunization. Immunol Lett 2007;109:13-20.
8. Inoue J, Aramaki Y. Toll-like receptor-9 expression induced by tape-stripping triggers on effective immune response with CpG-oligodeoxynucleotides. Vaccine 2007;25:1007-13.
9. Arora A, Prausnitz MR, Mitragotri S. Micro-scale devices for transdermal drug delivery. Int J Pharm 2008;364:227-36.
10. Gudmundsdotter L, Wahren B, Haller BK, Boberg A, Edbäck U, Bernasconi D, et al. Amplified antigen-specific immune responses in HIV-1 infected individuals in a double blind DNA immunization and therapy interruption trial. Vaccine 2011;29(33):5558-66.
11. Foldvari M, Badea I, Kumar P, Wettig S, Batta R, King MJ, et al. Biphasic vesicles for topical delivery of interferon alpha in human volunteers and treatment of patients with human papillomavirus infections. Curr Drug Deliv 2011;8:307-19.

12. Sprott GD, Patel GB, Makabi-Panzu BH, Tolson DL. Archaeosomes, archaeosomes containing coenzyme Q10, and other types of liposomes containing coenzyme Q10 as adjuvants and as delivery vehicles. European Patent 0 869 773 B1 WO 1997/022333 1997.

13. Krishnan L, Sad S, Patel GB, Sprott GD. The potent adjuvant activity of archaeosomes correlates to the recruitment and activation of macrophages and dendritic cells in vivo. J Immunol 2001;166:1885-93.

14. Nordly P, Korsholm KS, Pedersen EA, Khilji TS, Franzyk H, Jorgensen L, et al. Incorporation of a synthetic mycobacterial monomycoloyl glycerol analogue stabilizes dimethyldioctadecylammonium liposomes and potentiates their adjuvant effect in vivo. Eur J Pharm Biopharm 2011;77:89-98.

15. Dudani R, Chapdelaine Y, van Faassen H, Smith DK, Shen H, Krishnan L, et al. Preexisting inflammation due to *Mycobacterium bovis* BCG infection differentially modulates T-cell priming against a replicating or nonreplicating immunogen. Infect Immun 2002;70:1957-64.

16. Stan AC, Casares S, Brumeanu TD, Klinman DM, Bona CA. CpG motifs of DNA vaccines induce the expression of chemokines and MHC Class II molecules on myocytes. Eur J Immunol 2001;31:301-10.

17. Lambert PH, Laurent PE. Intradermal vaccine delivery: will new delivery systems transform vaccine administration? Vaccine 2008;26:3197-208.

18. Patel GB, Zhou H, Ponce A, Chen W. Mucosal and systemic immune responses by intranasal immunization using archaeal lipid-adjuvanted vaccines. Vaccine 2007;25:8622-36.

19. Gonzalez RO, Higa LH, Cutrullis RA, Bilen M, Morelli I, Roncaglia DI, et al. Archaeosomes made of *Halorubrum tebenquichense* total polar lipids: a new source of adjuvancy. BMC Biotechnol 2009;9:71-83.

20. Kates MKS. Protocol 5: Isoprenoids and polar lipids of extreme halophiles. In: DSaF EM, editor. Archaea. A laboratory manual. Halophiles. New York: Cold Spring Harbor Laboratory Press; 1995. p. 35-53.

21. Bötcher CJF, van Gent CM, Pries C. A rapid and sensitive submicro phosphorus determination. Anal Chim Acta 1961;24:203-4.

22. Fry DW, White JC, Goldman ID. Rapid separation of low molecular weight solutes from liposomes without dilution. Anal Biochem 1978;90:809-15.

23. Lovdahl MJ, Pietrzyk DJ. Anion-exchange separation and determination of bisphosphonates and related analytes by post-column indirect fluorescence detection. J Chromatogr A 1999;850:143-52.

24. Blight EG, Dyer WJ. A rapid method of total lipid extraction and purification. Can J Biochem Physiol 1959;37:911-7.

25. Bradford MM. A rapid and sensitive method for the quantitation of microgram quantities of protein utilizing the principle of protein-dye binding. Anal Biochem 1976;72:248-54.

26. van den Bergh BA, Wertz PW, Junginger HE, Bouwstra JA. Elasticity of vesicles assessed by electron spin resonance, electron microscopy and extrusion measurements. Int J Pharm 2001;217:13-24.

27. Cevc G. Material transport across permeability barriers by means of lipid vesicles. In: Lipowsky RSE, editor. Handbook of Biological Physics. Amsterdam: Elsevier; 1995. p. 465-90.

28. Montanari J, Maidana C, Esteva MI, Salomon C, Morilla MJ, Romero EL. Sunlight triggered photodynamic ultradeformable liposomes against *Leishmania braziliensis* are also leishmanicidal in the dark. J Control Release 2010;147:368-76.

29. Moreau MF, Guillet C, Massin P, Chevalier S, Gascan H, Baslé MF, et al. Comparative effects of five bisphosphonates on apoptosis of macrophage cells in vitro. Biochem Pharmacol 2007;73:718-23.

30. Stratis A, Pasparakis M, Rupec RA, Markur D, Hartmann K, Scharffetter-Kochanek K, et al. Pathogenic role for skin macrophages in a mouse model of keratinocyte-induced psoriasis-like skin inflammation. J Clin Invest 2006;116:2094-104.

31. Sallusto F. Origin and migratory properties of dendritic cells in the skin. Curr Opin Allergy Clin Immunol 2001;1:441-8.

32. Romero EL, Morilla MJ. Topical and mucosal liposomes for vaccine delivery. Wiley Interdiscip Rev Nanomed Nanobiotechnol 2011;3:356-75.

33. Cevc G, Vierl U. Nanotechnology and the transdermal route: a state of the art review and critical appraisal. J Control Release 2010;141:277-99.

34. Sprott GD. Structures of archaebacterial membrane lipids. J Bioenerg Biomembr 1992;24:555-66.

35. De Rosa M, Tricone A, Nicolaus B, Gambacorta A. Archaeabacteria: lipids, Membranes Structures and Adaptations to Environmental Stresses. In: di Prisco G, editor. Life Under Extreme Conditions. New York: Springer; 1991. p. 61-78.

36. Gurnani K, Kennedy J, Sad S, Sprott GD, Krishnan L. Phosphatidylserine receptor-mediated recognition of archaeosome adjuvant promotes endocytosis and MHC class I cross-presentation of the entrapped antigen by phagosome-to-cytosol transport and classical processing. J Immunol 2004;173:566-78.

37. Krishnan L, Sad S, Patel GB, Sprott GD. Archaeosomes induce long-term CD81 cytotoxic T cell response to entrapped soluble protein by the exogenous cytosolic pathway, in the absence of CD41 T cell help1. J Immunol 2000;165:5177-85.

38. Hoffmann PR, Kench JA, Vondracek A, Kruk E, Daleke DL, Jordan M, et al. Interaction between phosphatidylserine and the phosphatidylserine receptor inhibits immune responses in vivo. J Immunol 2005;174:1393-404.

39. Sprott GD, Sad S, Fleming LP, Dicaire C, Patel GB, Krishnan L. Archaeosomes varying in lipid composition differ in receptor-mediated endocytosis and differentially adjuvant immune responses to entrapped antigen. Archaea 2003;1:151-64.

40. Krishnan L, Sprott GD. Archaeosome adjuvants: Immunological capabilities and mechanism(s) of action. Vaccine 2008;26:2043-55.

41. Eckburg PB, Lepp PW, Relman DA. Archaea and their potential role in human disease. Infect Immun 2003;71:591-6.

42. Pulendran B, Palucka K, Banchereau J. Sensing pathogens and tuning immune responses. Science 2001;293:253-6.

43. Krishnan L, Gurnani K, Dicaire CJ, van Faassen H, Zafer A, Kirschning CJ, et al. Rapid clonal expansion and prolonged maintenance of memory CD8+ T cells of the effector (CD44highCD62Llow) and central (CD44highCD62Lhigh) phenotype by an archaeosome adjuvant independent of TLR2. J Immunol 2007;178:2396-406.

44. de la Salle H, Mariotti S, Angenieux C, Gilleron M, Garcia-Alles L-F, Malm D, et al. Assistance of microbial glycolipid antigen processing by CD1e. Science 2005;310:1321-4.

45. McGreal EP, Rosas M, Brown GD, Zamze S, Wong SYC, Gordon S, et al. The carbohydrate-recognition domain of Dectin-2 is a C-type lectin with specificity for high mannose. Glycobiology 2006;16:422-30.

46. Sprott GD, Dicaire CJ, Côtè J-P, Whitfield DM. Adjuvant potential of archaeal synthetic glycolipid mimetics critically depends on the glyco head group structure. Glycobiology 2008;18:559-65.

47. Whitfield DM, Eichler EE, Sprott GD. Synthesis of archaeal glycolipid adjuvants—what is the optimum number of sugars? Carbohydr Res 2008;343:2349-60.

48. Kamekura M, Kates M. Structural diversity of membrane lipids in members of Halobacteriaceae. Biosci Biotechnol Biochem 1999;63:969-72.